Tight information bounds for spontaneous-emission-lifetime resolution of quantum sources with varied spectral purity

Cheyenne S. Mitchell and Mikael P. Backlund*

Department of Chemistry and Illinois Quantum Information Science and Technology Center, University of Illinois at Urbana-Champaign, Urbana, Illinois 61801, USA

(Received 9 May 2023; accepted 18 July 2023; published 11 August 2023)

We generalize the theory of resolving a mixture of two closely spaced spontaneous emission lifetimes to include pure dephasing contributions to decoherence, leading to the resurgence of Rayleigh's curse at small lifetime separations. Considerable resolution enhancement remains possible when lifetime broadening is more significant than that due to pure dephasing. In the limit that lifetime broadening dominates, one can achieve super-resolution either by a tailored one-photon measurement or by Hong-Ou-Mandel interferometry. We describe conditions for which either choice is superior.

DOI: 10.1103/PhysRevA.108.023712

I. INTRODUCTION

A recent quantum-inspired analysis of the age-old problem of spatially resolving mutually incoherent optical point sources revealed conditions under which the precision of such a measurement can surpass the classical limit [1,2]. The authors showed that the quantum Fisher information (QFI) associated with estimation of the separation between two such point sources remains constant as the separation goes to zero, even as the classical Fisher information (CFI) associated with direct imaging vanishes in the same limit (dubbed "Rayleigh's curse"). A flurry of subsequent studies has since built on the theory [3–26] and experimentally demonstrated advantages in model imaging systems [27–36]. The basic idea has also been translated from position-momentum to time-frequency resolution [37–40]. In this spirit, we recently reported quantum limits associated with the estimation, resolution, and discrimination of optical spontaneous emission lifetimes [41].

An important contingent of this body of research has presented caveats to the theory that effectively temper one's ability to surpass Rayleigh's curse subject to certain experimental realities. Quantitatively, these caveats cause the QFI to eventually scale to zero as the separation becomes sufficiently small. Imperfect knowledge of the centroid position of the two sources is one such caveat that was explicitly noted from the beginning [1,42]. A mode-sorting measurement that would otherwise saturate the bound yields equivalent trends under misalignment or in the presence of crosstalk [43–45]. Various other nuisance parameters [46–51] or additional sources of noise [52–55] can lead to similar mitigation. In this paper, we detail another such caveat that is specifically relevant to the resolution of optical spontaneous-emission-lifetime mixtures. Namely, diminished spectral purity of the collected photons leads to a lowering of the associated QFI, eventually recovering the classical bound associated with direct measurement via time-correlated single-photon counting (TCSPC). We quantify the relation between spectral purity and QFI for this system, and show that a significant resolution enhancement remains possible in the case that lifetime broadening is more significant than broadening due to pure dephasing. In the limit of high spectral purity we consider the prospect of attaining super-resolution via Hong-Ou-Mandel (HOM) interference measurements [56] on subsequently emitted photons and compare performance to a tailored one-photon measurement scheme.

II. RESULTS AND DISCUSSION

For the sake of completeness, we begin this section by reintroducing the physical model and summarizing salient results from Ref. [41]. A two-level system initially prepared in its excited state and embedded in electromagnetic vacuum will eventually relax to its ground state, leaving the field in a one-photon state. For simplicity we suppose only a single polarization and transverse mode is possibly occupied just after the collecting aperture. Invoking the Wigner-Weisskopf approximation [57], the relevant one-photon state is taken as

$$|\psi_\tau(\omega)\rangle = \int_{-\infty}^{\infty} d\omega' \frac{1/\sqrt{2\pi\tau}}{(\omega'-\omega)+i/(2\tau)} a^\dagger(\omega')|0\rangle, \quad (1)$$

where ω is the photon's mean frequency, τ is the lifetime of the emitter, $a^\dagger(\omega')$ is the creation operator for the indicated mode, and $|0\rangle$ is the electromagnetic vacuum. We can alternatively express $|\psi_\tau\rangle$ in terms of the Fourier-transformed creation operator [58] (up to a global phase):

$$|\psi_\tau(\omega)\rangle = \int dt\ \psi_\tau(t;\omega) a^\dagger(t)|0\rangle = \int dt\ \psi_\tau(t;\omega)|t\rangle, \quad (2)$$

with $a^\dagger(t)$ the creation operator for the denoted temporal mode and

$$\psi_\tau(t;\omega) = \frac{H(t)}{\sqrt{\tau}} e^{-i\omega t} e^{-t/2\tau}, \quad (3)$$

*mikaelb@illinois.edu

where $H(t)$ is the Heaviside step function defined by $H(t \geqslant 0) = 1$ and $H(t < 0) = 0$. The definition of time t is shifted to compensate for the finite distance between emitter and detector, such that the time window of interest begins at $t = 0$.

Measurement of τ is a frequently encountered experimental objective, as this parameter can depend sensitively on the emitter's local environment. The most commonly employed experimental technique for such measurements is TCSPC, which entails directly measuring the distribution of delay times between pairs of excitation pulses and photodetection events. In Ref. [41] we showed that while TCSPC is optimal for the task of estimating a single lifetime, its performance quickly deteriorates when tasked with resolving mixtures of lifetimes, e.g., due to a multicomponent ensemble of emitters or a single emitter fluctuating among different distinct states. We focused our analysis on the simplest such task, the resolution of two lifetimes τ_0 and τ_1 given a mixed single-photon state of the form

$$\rho = \tfrac{1}{2}|\psi_{\tau_0}(\omega)\rangle\langle\psi_{\tau_0}(\omega)| + \tfrac{1}{2}|\psi_{\tau_1}(\omega)\rangle\langle\psi_{\tau_1}(\omega)|. \tag{4}$$

Upon reparametrizing the problem in terms of the geometric mean lifetime $\bar{\tau} = \sqrt{\tau_0\tau_1}$ and square-root ratio of lifetimes $\varepsilon = \sqrt{\tau_1/\tau_0}$ (assuming, without loss of generality, that $\tau_1 > \tau_0$), we found that the conventional measurement scheme based on TCSPC suffers from an analog of Rayleigh's curse in that the CFI associated with estimation of ε vanishes in the limit $\varepsilon \to 1$. By contrast, the QFI associated with estimating ε attains its maximum in the same limit. We showed that this quantum bound is saturated by a projective measurement onto the basis of weighted Laguerre (WL) modes defined by

$$|\phi_n(\omega, \bar{\tau})\rangle = \int dt\, \phi_n(t; \omega, \bar{\tau})|t\rangle \tag{5}$$

with

$$\phi_n(t; \omega, \bar{\tau}) = \frac{H(t)}{\sqrt{\bar{\tau}}} e^{-i\omega t} e^{-t/2\bar{\tau}} L_n(t/\bar{\tau}), \tag{6}$$

where $L_n(\cdot)$ denotes the Laguerre polynomial of order n. Note that the optimality of the WL projective measurement relies on prior knowledge of $\bar{\tau}$, gleaned perhaps from an initial TCSPC measurement (TCSPC does well to preserve information on $\bar{\tau}$ at all separations). For convenience, in Appendix A we reproduce the QFI associated with measuring ε and the CFIs associated with measuring this parameter via TCSPC, WL projection with perfect knowledge of $\bar{\tau}$, and WL projection with various degrees of imperfect knowledge of $\bar{\tau}$. In Ref. [41], we considered possible routes to experimental realization of WL projection as well as approximating interferometric schemes that outperform TCSPC.

Though it provides a useful starting point, the model underlying Eq. (4) employs several simplifying suppositions. In the current paper we will focus on one of these suppositions in particular: that the constituent single-lifetime states ρ_{τ_0} and ρ_{τ_1} are of unit purity, corresponding to photons whose spectral linewidths are lifetime limited. In realistic systems one must contend with (often dominant) incoherent contributions to the spectral linewidth due to inhomogeneous broadening (for emitter ensembles) and/or spectral diffusion (for single emitters). One typically has to work hard to produce lifetime-limited photons, either by freezing out sources of dephasing [59] or by engineering accelerated emission rates [60].

Here we amend our model such that the collected single-photon state is given by

$$\bar{\rho} = \tfrac{1}{2}(\bar{\rho}_{\tau_0} + \bar{\rho}_{\tau_1}), \tag{7}$$

where the overbar denotes incoherent averaging over a spectral density function $P(\omega)$ such that

$$\bar{\rho}_\tau = \int d\omega P(\omega)|\psi_\tau(\omega)\rangle\langle\psi_\tau(\omega)| \tag{8}$$

for $\tau \in \{\tau_0, \tau_1\}$. This simple phenomenological model [61] is sufficient to capture the effects we highlight below, though it neglects possible relations between the width of $P(\omega)$ and the lifetime that can arise depending on the physical origins of the contributions to decoherence [62]. To isolate the resolution problem, we assume $\bar{\tau}$ is known and set out to calculate $\mathcal{K}_\varepsilon$, the QFI associated with ε, for various choices of $P(\omega)$. We take $P(\omega)$ to be centered about some known frequency $\omega_0 > 0$ such that $P(\omega) = P_0(\omega - \omega_0)$, where $P_0(\omega)$ is centered at $\omega = 0$. The QFI is given by

$$\mathcal{K}_\varepsilon = \mathrm{Tr}\big(\mathcal{L}_\varepsilon^2 \bar{\rho}\big), \tag{9}$$

where $\mathcal{L}_\varepsilon$ is the symmetric logarithmic derivative (SLD) operator defined implicitly via

$$\partial_\varepsilon \bar{\rho} = \tfrac{1}{2}(\mathcal{L}_\varepsilon \bar{\rho} + \bar{\rho}\mathcal{L}_\varepsilon). \tag{10}$$

The SLD can be computed explicitly by first diagonalizing $\bar{\rho}$ such that

$$\bar{\rho} = \sum_k D_k |k\rangle\langle k| \tag{11}$$

and then equating

$$\mathcal{L}_\varepsilon = \sum_{k,k';D_k+D_{k'}\neq 0} \frac{2}{D_k + D_{k'}} \langle k|\partial_\varepsilon \bar{\rho}|k'\rangle\, |k\rangle\langle k'|. \tag{12}$$

To facilitate convergence we began our calculations by expressing $\bar{\rho}$ in the discrete basis of exponentially weighted Laguerre polynomials $|\phi_n(\omega_0, \bar{\tau})\rangle$ defined according to Eqs. (5) and (6). We show in Appendix B that matrix elements in this basis are given by

$$\langle\phi_n|\bar{\rho}_\tau|\phi_m\rangle = \frac{1}{\tau\bar{\tau}} \int d\omega \left\{ \frac{P_0(\omega)}{\omega^2 + \Gamma_+^2/4} \times \left[\frac{\Gamma_-/2 + i\omega}{\Gamma_+/2 + i\omega}\right]^n \left[\frac{\Gamma_-/2 - i\omega}{\Gamma_+/2 - i\omega}\right]^m \right\}, \tag{13}$$

where

$$\Gamma_\pm = \frac{1}{\tau} \pm \frac{1}{\bar{\tau}}. \tag{14}$$

For certain choices of $P_0(\omega)$ the integral in Eq. (13) might be analytically calculable via complex contour integration. In any case, it can be readily calculated numerically upon specifying $P_0(\omega)$. For the ensuing calculations we considered Gaussian broadening with spectral width parameter σ such that

$$P_0(\omega) = \frac{1}{\sqrt{2\pi\sigma^2}} e^{-\omega^2/2\sigma^2}. \tag{15}$$

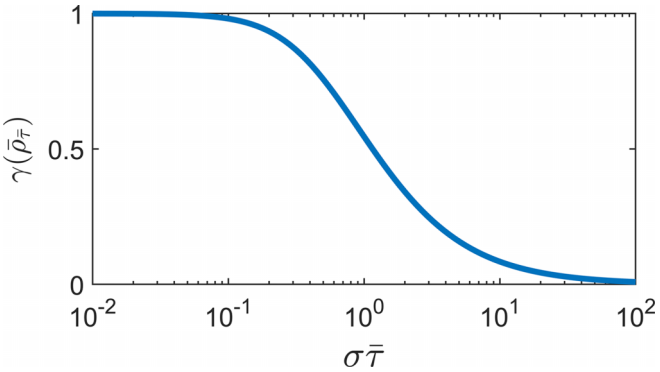

FIG. 1. Purity of the limiting state $\bar{\rho}_{\bar{\tau}}$ as a function of the product $\sigma\bar{\tau}$.

Comparison of σ and $1/\bar{\tau}$ determines the relative importance of lifetime broadening vs pure dephasing. Equivalently, the product $(\sigma\bar{\tau})$ specifies the purity (Fig. 1),

$$\gamma(\bar{\rho}_{\bar{\tau}}) = \mathrm{Tr}\big(\bar{\rho}_{\bar{\tau}}^2\big) = \frac{1}{\sqrt{4\pi}}\int_{-\infty}^{\infty} d\Omega\, \frac{e^{-\Omega^2/4}}{1+(\sigma\bar{\tau}\Omega)^2}, \tag{16}$$

of the limiting state:

$$\bar{\rho}_{\bar{\tau}} = \lim_{\varepsilon\to 1}\bar{\rho}. \tag{17}$$

In the limit $\sigma \ll 1/\bar{\tau}$ we expect lifetime broadening to dominate and for the problem to revert to that of resolving τ_0 and τ_1 given the state in Eq. (4) such that $\mathcal{K}_\varepsilon = \mathcal{K}_\varepsilon^{(\max)}$. In the limit $\sigma \gg 1/\bar{\tau}$ pure dephasing dominates and we expect $\mathcal{K}_\varepsilon = \mathcal{J}_\varepsilon^{(\mathrm{TCSPC})}$, i.e., the QFI should asymptotically approach the CFI for TCSPC. This fact can be appreciated by inspection of the matrix elements of $\bar{\rho}_\tau$ in the temporal mode basis:

$$\langle t|\bar{\rho}_\tau|t'\rangle = \frac{H(t)H(t')}{\tau} e^{-(t+t')/2\tau} e^{-i\omega_0(t-t')} e^{-(t-t')^2\sigma^2/2}. \tag{18}$$

The effect of fixing τ and taking $\sigma\to\infty$ in Eq. (18) is to kill the off-diagonal elements of the matrix, leaving only populations which coincide with the outcome probability density of a TCSPC measurement:

$$\langle t|\bar{\rho}_\tau|t\rangle = \frac{H(t)}{\tau} e^{-t/\tau}. \tag{19}$$

Equation (19) implies that the outcome of a TCSPC measurement is independent of σ, though we note that this is a consequence of our phenomenological model which treats σ and τ separately. Figure 2 shows computed values of $\mathcal{K}_\varepsilon$ for $\sigma = 0.01/\bar{\tau}$, $0.1/\bar{\tau}$, and $1/\bar{\tau}$ (solid lines). The gray shaded region is bounded above by $\mathcal{K}_\varepsilon^{(\max)}$ and below by $\mathcal{J}_\varepsilon^{(\mathrm{TCSPC})}$. For $\sigma \ll 1/\bar{\tau}$ we see that indeed $\mathcal{K}_\varepsilon \approx \mathcal{K}_\varepsilon^{(\max)}$ over most of the domain, but for ε sufficiently close to 1 the QFI begins to trend back down toward zero, indicating the resurgence of Rayleigh's curse. Figure 3 displays the same data as in Fig. 2 on a semilogarithmic scale. Close inspection reveals that despite the resurgence of Rayleigh's curse, orders-of-magnitude resolution enhancement over TCSPC remains possible at ε close to 1 and $\sigma < 0.1/\bar{\tau}$ [$\gamma(\bar{\rho}_{\bar{\tau}}) \gtrapprox 0.98$].

The color-coded dashed lines in Figs. 2 and 3 mark the calculated CFIs, $\mathcal{J}_\varepsilon^{(\mathrm{WL})}$, associated with a projective measurement onto weighted Laguerre modes $\{|\phi_n(\omega_0,\bar{\tau})\rangle\langle\phi_n(\omega_0,\bar{\tau})|\}_n$ truncated at $n_{\max} = 100$. Actually only the single mode corresponding to $n = 1$ is required to recover >87% and >99% of the available information near $\varepsilon = 1.05$ for $\sigma = 0.01/\bar{\tau}$ and $0.1/\bar{\tau}$, respectively. For $\sigma = 1/\bar{\tau}$ a projective measurement onto the first 100 WL modes is evidently far from optimal, as the dark blue dashed line falls well below the gray region. For $\sigma \geqslant 1/\bar{\tau}$ TCSPC does well to recover the available information; in this case, the most obvious measurement is the correct one. Figure 4 depicts similar data for the borderline case of $\sigma = 0.25/\bar{\tau}$ [$\gamma(\bar{\rho}_{\bar{\tau}}) \approx 0.905$]. Here we scale the Fisher information curves by $\mathcal{J}_\varepsilon^{(\mathrm{TCSPC})}$. A modest information gain just

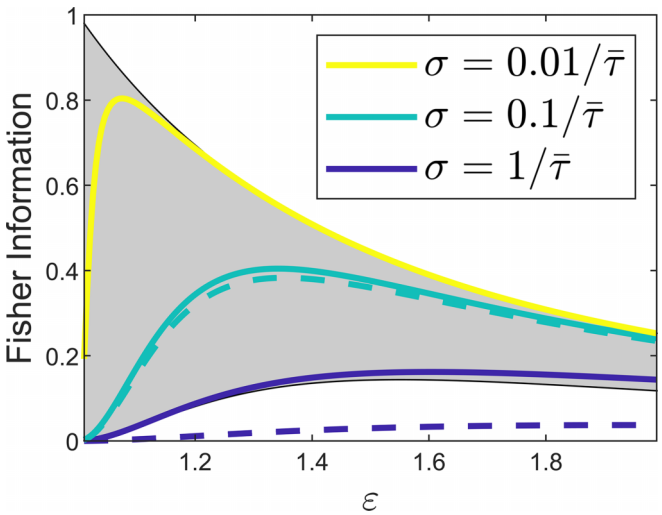

FIG. 2. Fisher information associated with estimation of ε. The gray region is bounded above by the QFI in the limit $P_0(\omega) \to \delta(\omega)$ and below by the CFI associated with TCSPC. Fisher information which falls within the gray region therefore indicates a potential advantage over TCSPC. Solid colored lines demarcate the calculated QFI at varying degrees of spectral purity. Dashed colored lines indicate the CFI associated with projective measurement onto a set of WL modes as described in the text. The yellow dashed line is obscured as it overlaps almost completely with the yellow solid line.

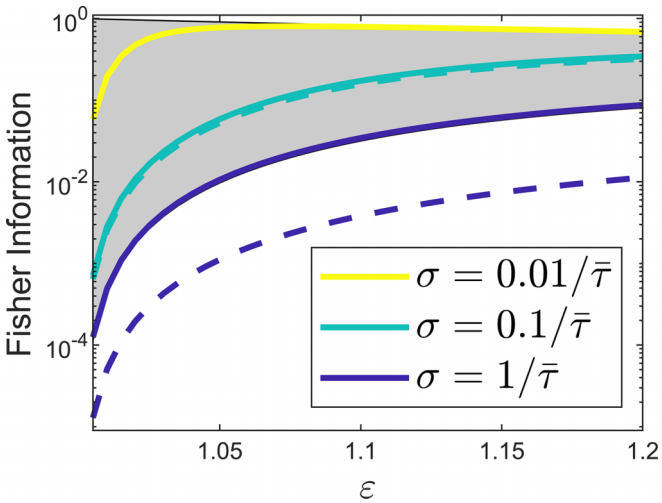

FIG. 3. The same data as in Fig. 2 presented on a semilogarithmic scale.

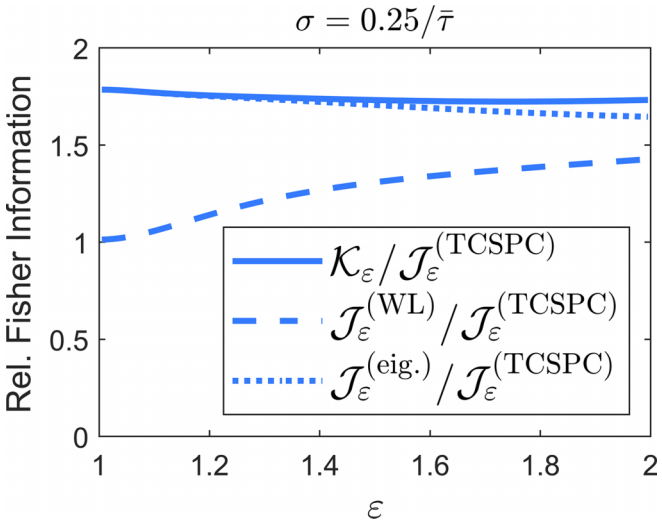

FIG. 4. QFI (solid), CFI for WL projection (dashed), and CFI for optimal measurement near $\varepsilon = 1$ (dotted) associated with the borderline case $\sigma = 0.25/\bar{\tau}$. Values are scaled by CFI of TCSPC.

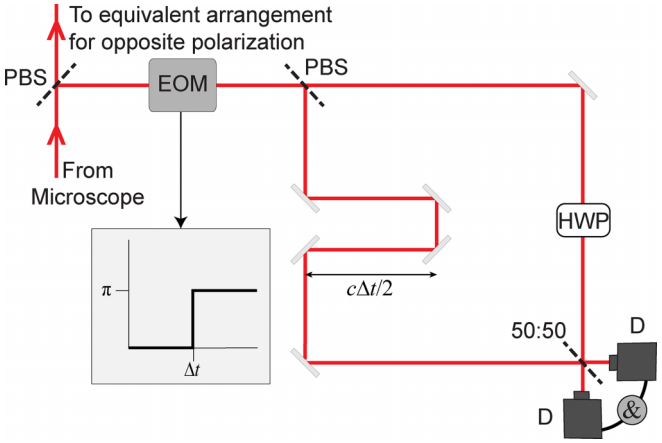

FIG. 5. Proposed setup for resolving lifetimes via two-photon interferometry, including polarizing beam splitter (PBS), electro-optic modulator (EOM), half-wave plate (HWP), nonpolarizing 50:50 beam splitter, and coincidence detectors (D). The portion depicted here modulates the component of the emission that is s polarized with respect to the first PBS. An analogous setup can be built on the other side to measure the p-polarized component.

under $2\times$ is available in this case, but it is not recovered by a measurement in the WL basis. For estimation of the single parameter ε, an optimal measurement can be constructed by projection onto the eigenstates of $\mathcal{L}_\varepsilon$. We calculate the performance of such a measurement for one choice of ε by numerically diagonalizing $\mathcal{L}_\varepsilon$ after expressing $\bar{\rho}$ in the WL basis up to $n_{\max} = 100$ (dotted line in Fig. 4).

The preceding analysis puts a finer point on exactly what quantum feature is needed to significantly surpass the resolution performance of TCSPC, namely, that coherences in the temporal mode basis must be preserved. Maximal information gain is possible in the idealized case that $\sigma \ll 1/\bar{\tau}$, for which subsequently collected photons are otherwise indistinguishable in the limit $\varepsilon \to 1$. It is therefore apparent that in the limit $\sigma \to 0$ one has a choice between performing a tailored one-photon measurement and performing a multiphoton interferometry measurement that exploits their near indistinguishability. Having recognized this, we next analyze the lifetime-resolving power of a two-photon Hong-Ou-Mandel-type measurement, which has been shown previously to provide certain advantages in the context of the spatial resolution problem [63]. HOM interferometry has been employed previously to quantify photon indistinguishability and discriminate mechanisms of decoherence in the emission of quantum sources [62,64–66]. Here we flip this problem around to show that if one knows somehow that the dominant source of indistinguishability is a mixture of lifetimes, then the HOM measurement can super-resolve these parameters.

We consider a hypothetical experiment using the apparatus depicted in Fig. 5. Subsequent excitation pulses are separated in time by an interval Δt significantly longer than $\bar{\tau}$ such that emission in the window between the two pulses and emission in the window after the second pulse are uncorrelated. We begin with a two-photon state of the form $\rho^{(2)} = \rho \otimes \rho$, where ρ is the one-photon state defined in Eq. (4). The QFI associated with ε for this product state is simply twice that of ρ, i.e., $\mathcal{K}_\varepsilon^{(2)} = 2\mathcal{K}_\varepsilon^{(\max)}$. The first collected photon is sent along one path and the second is sent along another by implementation of a switch synced with the second excitation pulse. This could be achieved, for example, by digitally switching an electro-optic modulator just before a polarizing beam splitter [67]. The path of the first collected photon contains a delay stage to compensate the interpulse duration Δt. The path of the second collected photon contains a half-wave plate to rotate the polarization to match that of the first photon. Then the two photons are brought together at either input port of a 50:50 beam splitter. There are four equally probable possibilities for the pair of lifetimes, which we denote (τ_0, τ_0), (τ_0, τ_1), (τ_1, τ_0), and (τ_1, τ_1). If we have (τ_0, τ_0) or (τ_1, τ_1) then the two photons are indistinguishable, and they will either both exit via port 1 or both exit via port 2. If instead we draw (τ_0, τ_1) or (τ_1, τ_0), there arises a small ε-dependent probability that the two photons emerge from opposite exit ports. By repeating the experiment and counting coincidences one can generate an estimate of ε. Our analysis detailed in Appendix C shows that this measurement scheme recovers half of the available information, i.e., $\mathcal{J}_\varepsilon^{(\&)} = \mathcal{K}_\varepsilon^{(2)}/2$, when $\varepsilon \to 1$. Rayleigh's curse is successfully circumvented by this HOM measurement in the limiting case where $\sigma \to 0$. From the preceding analysis we can also conclude that given the choice between an optimal one-photon measurement and the described two-photon coincidence measurement, the former is superior in terms of information per photon detected. If, however, one has a choice between the two-photon coincidence measurement and a suboptimal one-photon measurement scheme that only recovers a fraction $\xi < 1$ of the available information per photon detected (i.e., $\mathcal{J}_{\varepsilon\to 1}^{(\xi)} = \xi\mathcal{K}_{\varepsilon\to 1}^{(\max)}$, as in the cases of the single-photon interferometers presented in Ref. [41]), then which scheme is superior depends on whether ξ is greater or less than $1/2$.

To this point in the analysis we have assumed that one photon is certainly collected and detected within the interval immediately following each excitation pulse. Under realistic

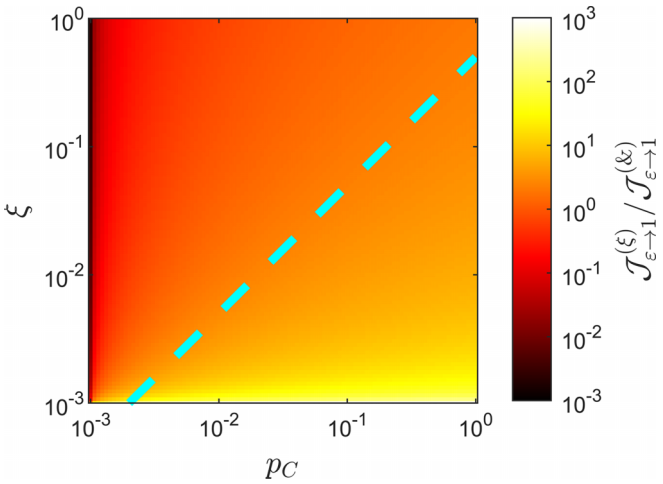

FIG. 6. Comparison of the CFIs for ε estimation conveyed by a one-photon measurement that obtains a fraction ξ of the QFI vs the HOM measurement depicted in Fig. 5, as a function of ξ and photon collection probability p_C. The cyan dashed line marks the contour along which the two are equal, corresponding to $\xi = p_C/2$.

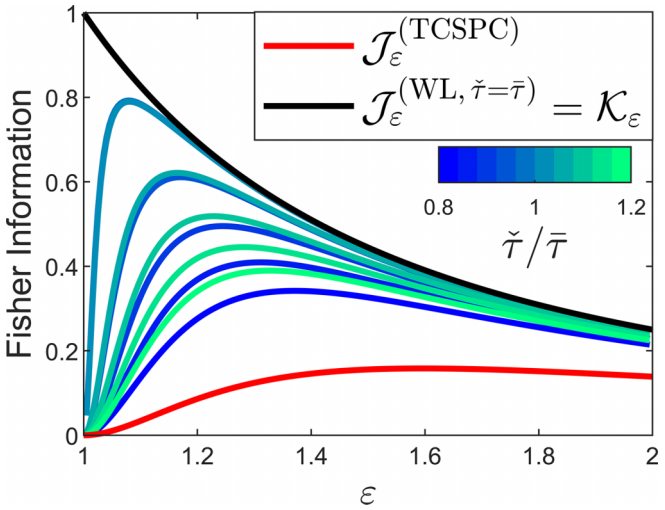

FIG. 7. Fisher information for ε estimation given the state defined by Eq. (4), as originally reported in Ref. [41]. The top, black line traces the QFI, which coincides with the CFI of a projective measurement onto a set of WL modes $\{\phi_n(t;\bar{\tau})\}_n$ assuming prior knowledge of $\bar{\tau}$. The bottom, red line indicates the CFI associated with TCSPC. The lines in between correspond to projective measurements onto sets of shifted WL modes $\{\phi_n(t;\check{\tau})\}_n$ with various mismatched mean lifetimes $\check{\tau} \neq \bar{\tau}$. Similar to the performance of centroid-mismatched SPADE vis-à-vis spatial resolution [1], the effect of mismatch is a diminished (and eventually vanishing) CFI at sufficiently small ε.

conditions, losses of various origins must be carefully considered. Setting aside measurement-dependent losses for now, a nonunit measurement-independent probability of collection, p_C, persists due to the probability of absorption, the quantum yield of the emitter, and the limited numerical aperture of the objective. In practice it is likely that $p_C \ll 1$. The relevant state of the field immediately following an excitation pulse is then

$$\rho' = (1 - p_C)|\mathrm{vac}\rangle\langle\mathrm{vac}| + p_C\rho. \tag{20}$$

The collective state of two such intervals, $\rho' \otimes \rho'$, contains two photons only with probability p_C^2, meaning that it is less likely that a pair of excitation pulses will produce a successful HOM measurement event than they will produce at least one successful one-photon measurement event. In this case a suboptimal one-photon measurement with efficiency ξ is superior to the two-photon coincidence scheme if $\xi > p_C/2$. Figure 6 depicts the ratio $\mathcal{J}_{\varepsilon\to1}^{(\xi)}/\mathcal{J}_{\varepsilon\to1}^{(\&)}$ for various choices of ξ and p_C.

Of course, additional measurement-dependent losses determined by the particular arrangement of optical elements placed between the objective lens and the detector will also affect this comparison. Imbalance due to, e.g., beam splitter asymmetry or imperfect polarization rotation will further penalize interferometric measurement. We reserve a more thorough quantification of these effects for future work. The HOM scheme does offer a distinct potential advantage over super-resolving one-photon measurements in that the former does not require prior knowledge of the mean lifetime $\bar{\tau}$ to achieve super-resolution. This fact can be partly appreciated by inspection of Eq. (C10), in which common factors of $\bar{\tau}$ have canceled one another. Choices of when to pulse the electro-optic modulator and how long to make the delay line in Fig. 5 depend only on the time between excitation pulses, Δt, and so are independent of the precise value of $\bar{\tau}$ so long as it is safe to assume $\Delta t \gg \bar{\tau}$. By contrast, the correct choice of WL basis for an optimal one-photon measurement depends explicitly on $\bar{\tau}$, as estimated, e.g., from a preliminary TCSPC measurement. Projective measurement in a WL basis with mismatched $\check{\tau} \neq \bar{\tau}$ leads to reduced resolving performance (Fig. 7).

III. CONCLUSION

In conclusion, we have effectively tightened the quantum bounds associated with resolution of optical spontaneous emission lifetimes by incorporating pure dephasing contributions to the spectral linewidth. When lifetime broadening dominates, a significant information gain can be uncovered by an appropriately tailored one- or two-photon measurement. When pure dephasing dominates, the conventional TCSPC measurement cannot be beat. It appears that any finite degree of pure dephasing causes the resolution QFI to scale back to zero for ε sufficiently close to 1, indicating the eventual resurgence of the lifetime analog of Rayleigh's curse.

ACKNOWLEDGMENTS

We thank Y. Wang, S. Bogdanov, and E. Goldschmidt for helpful comments on the paper. This work was supported via startup funds provided by the Department of Chemistry and the School of Chemical Sciences at the University of Illinois at Urbana-Champaign.

APPENDIX A: SOME RELEVANT RESULTS FROM REF. [41]

In Fig. 7 we reproduce select results from Ref. [41].

APPENDIX B: DERIVATION OF EQ. (13)

Here we derive an integral expression for the matrix elements of density operator $\bar{\rho}_\tau$ in the basis of weighted Laguerre modes $|\phi_n(\omega_0, \bar{\tau})\rangle$ given by

$$|\phi_n(\omega_0, \bar{\tau})\rangle = \int dt\, \phi_n(t; \omega_0, \bar{\tau})|t\rangle \tag{B1}$$

with

$$\phi_n(t; \omega_0, \bar{\tau}) = \frac{H(t)}{\sqrt{\bar{\tau}}} e^{-i\omega_0 t} e^{-t/2\bar{\tau}} L_n(t/\bar{\tau}). \tag{B2}$$

We take

$$\bar{\rho}_\tau = \int d\omega\, P_0(\omega - \omega_0)\rho_\tau(\omega) \tag{B3}$$

with the pure state $\rho_\tau(\omega)$ given in the temporal mode basis by

$$\rho_\tau(\omega) = \int dt \int dt' \frac{H(t)H(t')}{\tau} e^{-i\omega(t-t')} e^{-(t+t')/2\tau} |t\rangle\langle t'|. \tag{B4}$$

Plugging Eq. (B4) into Eq. (B3) and reordering integrals gives

$$\bar{\rho}_\tau = \int dt \int dt' \left\{ \frac{H(t)H(t')}{\tau} e^{-(t+t')/2\tau} \times \left[\int d\omega\, e^{-i\omega(t-t')} P_0(\omega - \omega_0) \right] |t\rangle\langle t'| \right\}. \tag{B5}$$

Defining

$$\hat{P}_0(t) = \frac{1}{\sqrt{2\pi}} \int d\omega\, e^{-i\omega t} P_0(\omega) \tag{B6}$$

and making use of the shifting property of the Fourier transform gives

$$\bar{\rho}_\tau = \sqrt{2\pi} \int dt \int dt' \left\{ \frac{H(t)H(t')}{\tau} e^{-(t+t')/2\tau} \times e^{-i\omega_0(t-t')} \hat{P}_0(t - t') |t\rangle\langle t'| \right\}. \tag{B7}$$

Combining Eqs. (B1), (B2), and (B7) then yields an expression for the (n, m) matrix element of $\bar{\rho}_\tau$:

$$\langle\phi_n|\bar{\rho}_\tau|\phi_m\rangle = \sqrt{2\pi} \int dt \int dt' \left\{ \frac{H(t)H(t')}{\tau\bar{\tau}} e^{-\Gamma_+(t-t')/2} \times L_n(t/\bar{\tau}) L_m(t/\bar{\tau}) \hat{P}_0(t - t') \right\} \tag{B8}$$

where

$$\Gamma_\pm = \frac{1}{\tau} \pm \frac{1}{\bar{\tau}}. \tag{B9}$$

We define a set of functions

$$f_n(t) = H(t) e^{-\Gamma_+ t/2} L_n(t/\bar{\tau}) \tag{B10}$$

and rearrange integrals to obtain

$$\langle\phi_n|\bar{\rho}_\tau|\phi_m\rangle = \frac{\sqrt{2\pi}}{\tau\bar{\tau}} \int dt\, f_n(t) \left(\int dt'\, f_m(t') \hat{P}_0(t - t') \right). \tag{B11}$$

The integral over t' amounts to a convolution and so we can write

$$\langle\phi_n|\bar{\rho}_\tau|\phi_m\rangle = \frac{\sqrt{2\pi}}{\tau\bar{\tau}} \int dt\, f_n(t)[f_m * \hat{P}_0](t). \tag{B12}$$

The t integral is converted to an ω integral by application of Parseval's theorem:

$$\langle\phi_n|\bar{\rho}_\tau|\phi_m\rangle = \frac{\sqrt{2\pi}}{\tau\bar{\tau}} \int d\omega \hat{f}_n^*(\omega) \mathscr{F}\{f_m * \hat{P}_0\}(\omega), \tag{B13}$$

where $\mathscr{F}\{\cdot\}$ denotes the Fourier transform of the convolved function. Implementation of the convolution theorem plus some additional manipulation yields

$$\langle\phi_n|\bar{\rho}_\tau|\phi_m\rangle = \frac{2\pi}{\tau\bar{\tau}} \int d\omega \hat{f}_n^*(-\omega) \hat{f}_m(-\omega) P_0(\omega). \tag{B14}$$

The Fourier transform of f_n can be easily computed by recognizing the relation

$$\hat{f}_n(\omega) = \frac{1}{\sqrt{2\pi}} \mathscr{L}\{L_n(t/\bar{\tau})\}(s = \Gamma_+/2 + i\omega), \tag{B15}$$

where $\mathscr{L}\{\cdot\}(s)$ denotes the Laplace transform evaluated at complex frequency s. Laplace transforms of Laguerre polynomials have particularly simple forms [68], ultimately allowing us to conclude

$$\hat{f}_n(\omega) = \frac{1}{\sqrt{2\pi}(\Gamma_+/2 + i\omega)} \left(\frac{\Gamma_-/2 + i\omega}{\Gamma_+/2 + i\omega} \right)^n. \tag{B16}$$

Equation (13) follows directly from Eqs. (B16) and (B14).

APPENDIX C: ANALYSIS OF HOM MEASUREMENT

Here we derive the Fisher information with respect to estimation of ε for the two-photon interference measurement illustrated in Fig. 5. We consider the limiting case in which $\sigma \to 0$ and single-photon states reduce to

$$\rho = \tfrac{1}{2}|\psi_{\tau_0}\rangle\langle\psi_{\tau_0}| + \tfrac{1}{2}|\psi_{\tau_1}\rangle\langle\psi_{\tau_1}|. \tag{C1}$$

Just before the final 50 : 50 beam splitter depicted in Fig. 5, the relevant two-photon state can be written

$$\rho^{(2)} = \sum_{i,j\in\{0,1\}} \frac{1}{4} |\psi_{\tau_i}\psi_{\tau_j}\rangle\langle\psi_{\tau_i}\psi_{\tau_j}|, \tag{C2}$$

with

$$|\psi_{\tau_i}\psi_{\tau_j}\rangle = \int dt \int dt'\, \psi_{\tau_i}(t)\psi_{\tau_j}(t') a_1^\dagger(t) a_2^\dagger(t')|0\rangle, \tag{C3}$$

where $a_1^\dagger$ and $a_2^\dagger$ are the creation operators for the input modes of the beam splitter and $|0\rangle$ denotes the vacuum state. Thus $\rho^{(2)}$ corresponds to an equal-probability mixture of four pure input states. We calculate the outcome probabilities for each $|\Psi_{ij}^{(\mathrm{in})}\rangle = |\psi_{\tau_i}\psi_{\tau_j}\rangle$ separately before resumming. The beam splitter imparts the transformation:

$$a_1^\dagger(t) \to \frac{1}{\sqrt{2}}[a_3^\dagger(t) + i a_4^\dagger(t)], \tag{C4a}$$

$$a_2^\dagger(t) \to \frac{1}{\sqrt{2}}[i a_3^\dagger(t) + a_4^\dagger(t)], \tag{C4b}$$

where $a_3^\dagger$ and $a_4^\dagger$ are the creation operators for the output modes. The state $|\Psi_{ij}^{(\mathrm{in})}\rangle$ is transformed to $|\Psi_{ij}^{(\mathrm{out})}\rangle$ given by

$$\left|\Psi_{ij}^{(\mathrm{out})}\right\rangle = \int dt \int dt' \, \frac{\psi_{\tau_i}(t)\psi_{\tau_j}(t')}{2}[a_3^\dagger(t) + ia_4^\dagger(t)] \times [ia_3^\dagger(t') + a_4^\dagger(t')]|0\rangle. \tag{C5}$$

We consider the positive operator-valued measure $\{\hat{P}^{(\&)}, \hat{1} - \hat{P}^{(\&)}\}$ where $\hat{1}$ is the identity operator and $\hat{P}^{(\&)}$ is the coincidence projector defined by

$$\hat{P}^{(\&)} = \int dt'' \int dt''' \, a_3^\dagger(t'')a_4^\dagger(t''')|0\rangle\langle 0|a_4(t''')a_3(t''). \tag{C6}$$

Given output state $|\Psi_{ij}^{(\mathrm{out})}\rangle$, the probability of recording a coincidence is given by

$$p_{ij}^{(\&)} = \left\langle \Psi_{ij}^{(\mathrm{out})} \middle| \hat{P}^{(\&)} \middle| \Psi_{ij}^{(\mathrm{out})} \right\rangle, \tag{C7}$$

yielding

$$p_{ij}^{(\&)} = \tfrac{1}{2}\left(1 - \left|\langle \psi_{\tau_i} | \psi_{\tau_j} \rangle\right|^2\right). \tag{C8}$$

Clearly $p_{00}^{(\&)} = p_{11}^{(\&)} = 0$. For $i \neq j$,

$$p_{10}^{(\&)} = p_{01}^{(\&)} = \frac{1}{2}\left(1 - \frac{4\tau_0\tau_1}{(\tau_0+\tau_1)^2}\right). \tag{C9}$$

Given $\tau_0 = \bar{\tau}/\varepsilon$ and $\tau_1 = \bar{\tau}\varepsilon$ this reduces to

$$p_{10}^{(\&)} = p_{01}^{(\&)} = \frac{1}{2}\left(\frac{\varepsilon^2-1}{\varepsilon^2+1}\right)^2. \tag{C10}$$

Now, considering the mixed state defined in Eq. (C2), the overall probability of recording a coincidence is

$$p^{(\&)} = \sum_{i,j\in\{0,1\}} \frac{p_{ij}^{(\&)}}{4} = \frac{1}{4}\left(\frac{\varepsilon^2-1}{\varepsilon^2+1}\right)^2. \tag{C11}$$

The measurement outcome (coincidence vs noncoincidence) is a Bernoulli random variable with success rate $p^{(\&)}$. The Fisher information with respect to ε is given by

$$\mathcal{J}_\varepsilon^{(\&)} = \frac{1}{p^{(\&)}(1-p^{(\&)})}\left(\frac{dp^{(\&)}}{d\varepsilon}\right)^2 \tag{C12}$$

which simplifies to

$$\mathcal{J}_\varepsilon^{(\&)} = \frac{64\varepsilon^2}{(\varepsilon^2+1)^2(3\varepsilon+1)(\varepsilon+3)}. \tag{C13}$$

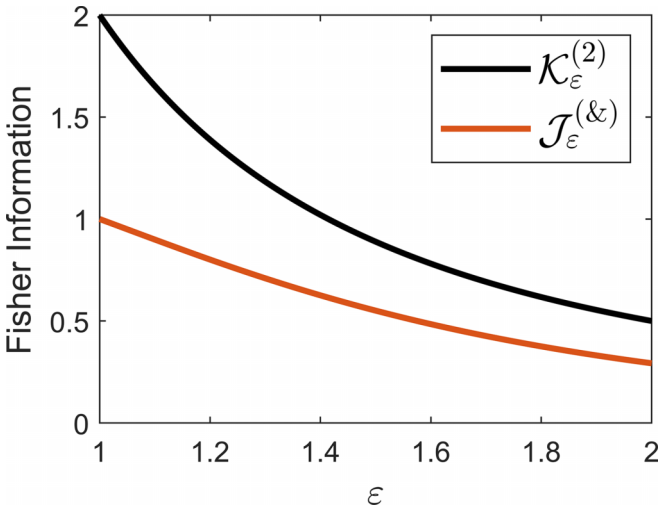

FIG. 8. QFI for lifetime resolution given the composite state $\rho^{(2)}$ compared to the CFI of a HOM measurement with coincidence counting.

Figure 8 plots both $\mathcal{J}_\varepsilon^{(\&)}$ and the QFI associated with estimating ε from the two-photon product state, $\mathcal{K}_\varepsilon^{(2)}$. In particular, for $\varepsilon \to 1$ we find $\mathcal{J}_\varepsilon^{(\&)} = \mathcal{K}_\varepsilon^{(2)}/2$.

[1] M. Tsang, R. Nair, and X.-M. Lu, Quantum Theory of Superresolution for Two Incoherent Optical Point Sources, Phys. Rev. X **6**, 031033 (2016).

[2] M. Tsang, Resolving starlight: A quantum perspective, Contemp. Phys. **60**, 279 (2019).

[3] R. Nair and M. Tsang, Far-Field Superresolution of Thermal Electromagnetic Sources at the Quantum Limit, Phys. Rev. Lett. **117**, 190801 (2016).

[4] R. Nair and M. Tsang, Interferometric superlocalization of two incoherent optical point sources, Opt. Express **24**, 3684 (2016).

[5] M. Tsang, Subdiffraction incoherent optical imaging via spatial-mode demultiplexing, New J. Phys. **19**, 023054 (2017).

[6] S. Z. Ang, R. Nair, and M. Tsang, Quantum limit for two-dimensional resolution of two incoherent optical point sources, Phys. Rev. A **95**, 063847 (2017).

[7] M. Tsang, Subdiffraction incoherent optical imaging via spatial-mode demultiplexing: Semiclassical treatment, Phys. Rev. A **97**, 023830 (2018).

[8] J. Řeháček, M. Paúr, B. Stoklasa, Z. Hradil, and L. L. Sánchez-Soto, Optimal measurements for resolution beyond the Rayleigh limit, Opt. Lett. **42**, 231 (2017).

[9] M. Tsang, Quantum limit to subdiffraction incoherent optical imaging, Phys. Rev. A **99**, 012305 (2019).

[10] S. Zhou and L. Jiang, Modern description of Rayleigh's criterion, Phys. Rev. A **99**, 013808 (2019).

[11] E. Bisketzi, D. Branford, and A. Datta, Quantum limits of localisation microscopy, New J. Phys. **21**, 123032 (2019).

[12] C. Lupo, Z. Huang, and P. Kok, Quantum Limits to Incoherent Imaging are Achieved by Linear Interferometry, Phys. Rev. Lett. **124**, 080503 (2020).

[13] F. Bao, H. Choi, V. Aggarwal, and Z. Jacob, Quantum-accelerated imaging of n stars, Opt. Lett. **46**, 3045 (2021).

[14] M. Bojer, Z. Huang, S. Karl, S. Richter, P. Kok, and J. von Zanthier, A quantitative comparison of amplitude versus intensity interferometry for astronomy, New J. Phys. **24**, 043026 (2022).

[15] C. Datta, Y. L. Len, K. Łukanowski, K. Banaszek, and M. Jarzyna, Sub-rayleigh characterization of a binary source by spatially demultiplexed coherent detection, Opt. Express **29**, 35592 (2021).
[16] M. R. Grace and S. Guha, Identifying Objects at the Quantum Limit for Superresolution Imaging, Phys. Rev. Lett. **129**, 180502 (2022).
[17] Z. Huang and C. Lupo, Quantum Hypothesis Testing for Exoplanet Detection, Phys. Rev. Lett. **127**, 130502 (2021).
[18] Z. Huang, C. Schwab, and C. Lupo, Ultimate limits of exoplanet spectroscopy: A quantum approach, Phys. Rev. A **107**, 022409 (2023).
[19] J. M. Jusuf and M. D. Lew, Towards optimal point spread function design for resolving closely spaced emitters in three dimensions, Opt. Express **30**, 37154 (2022).
[20] I. Karuseichyk, G. Sorelli, M. Walschaers, N. Treps, and M. Gessner, Resolving mutually-coherent point sources of light with arbitrary statistics, Phys. Rev. Res. **4**, 043010 (2022).
[21] H. Krovi, Superresolution at the quantum limit beyond two point sources, arXiv:2206.14788 (2022).
[22] S. Kurdzialek, Back to sources: The role of losses and coherence in super-resolution imaging revisited, Quantum **6**, 697 (2022).
[23] Z. Hradil, J. Řeháček, L. Sánchez-Soto, and B.-G. Englert, Quantum fisher information with coherence, Optica **6**, 1437 (2019).
[24] K. Liang, S. A. Wadood, and A. N. Vamivakas, Coherence effects on estimating general sub-rayleigh object distribution moments, Phys. Rev. A **104**, 022220 (2021).
[25] G. Sorelli, M. Gessner, M. Walschaers, and N. Treps, Moment-based superresolution: Formalism and applications, Phys. Rev. A **104**, 033515 (2021).
[26] Y. Wang, Y. Zhang, and V. O. Lorenz, Superresolution in interferometric imaging of strong thermal sources, Phys. Rev. A **104**, 022613 (2021).
[27] F. Yang, A. Tashchilina, E. S. Moiseev, C. Simon, and A. I. Lvovsky, Far-field linear optical superresolution via heterodyne detection in a higher-order local oscillator mode, Optica **3**, 1148 (2016).
[28] Z. S. Tang, K. Durak, and A. Ling, Fault-tolerant and finite-error localization for point emitters within the diffraction limit, Opt. Express **24**, 22004 (2016).
[29] P. Boucher, C. Fabre, G. Labroille, and N. Treps, Spatial optical mode demultiplexing as a practical tool for optimal transverse distance estimation, Optica **7**, 1621 (2020).
[30] S. A. Wadood, K. Liang, Y. Zhou, J. Yang, M. A. Alonso, X.-F. Qian, T. Malhotra, S. M. H. Rafsanjani, A. N. Jordan, R. W. Boyd, and A. N. Vamivakas, Experimental demonstration of superresolution of partially coherent light sources using parity sorting, Opt. Express **29**, 22034 (2021).
[31] Y. Zhou, J. Yang, J. D. Hassett, S. M. H. Rafsanjani, M. Mirhosseini, A. N. Vamivakas, A. N. Jordan, Z. Shi, and R. W. Boyd, Quantum-limited estimation of the axial separation of two incoherent point sources, Optica **6**, 534 (2019).
[32] W.-K. Tham, H. Ferretti, and A. M. Steinberg, Beating Rayleigh's Curse by Imaging Using Phase Information, Phys. Rev. Lett. **118**, 070801 (2017).
[33] M. Paúr, B. Stoklasa, Z. Hradil, L. L. Sánchez-Soto, and J. Řeháček, Achieving the ultimate optical resolution, Optica **3**, 1144 (2016).
[34] M. Paúr, B. Stoklasa, J. Grover, A. Krzic, L. L. Sánchez-Soto, Z. Hradil, and J. Řeháček, Tempering Rayleigh's curse with PSF shaping, Optica **5**, 1177 (2018).
[35] L. Santamaria, D. Pallotti, M. S. de Cumis, D. Dequal, and C. Lupo, Spatial-mode-demultiplexing for enhanced intensity and distance measurement, arXiv:2206.05246 (2023).
[36] H. Zhang, S. Kumar, and Y.-P. Huang, Super-resolution optical classifier with high photon efficiency, Opt. Lett. **45**, 4968 (2020).
[37] J. M. Donohue, V. Ansari, J. Řeháček, Z. Hradil, B. Stoklasa, M. Paúr, L. L. Sánchez-Soto, and C. Silberhorn, Quantum-Limited Time-Frequency Estimation through Mode-Selective Photon Measurement, Phys. Rev. Lett. **121**, 090501 (2018).
[38] S. De, J. Gil-Lopez, B. Brecht, C. Silberhorn, L. L. Sánchez-Soto, Z. Hradil, and J. Řeháček, Effects of coherence on temporal resolution, Phys. Rev. Res. **3**, 033082 (2021).
[39] V. Ansari, B. Brecht, J. Gil-Lopez, J. M. Donohue, J. Řeháček, Z. Hradil, L. L. Sánchez-Soto, and C. Silberhorn, Achieving the ultimate quantum timing resolution, PRX Quantum **2**, 010301 (2021).
[40] M. Shah and L. Fan, Frequency Superresolution with Spectrotemporal Shaping of Photons, Phys. Rev. Appl. **15**, 034071 (2021).
[41] C. S. Mitchell and M. P. Backlund, Quantum limits to resolution and discrimination of spontaneous emission lifetimes, Phys. Rev. A **105**, 062603 (2022).
[42] M. R. Grace, Z. Dutton, A. Ashok, and S. Guha, Approaching quantum-limited imaging resolution without prior knowledge of the object location, J. Opt. Soc. Am. A **37**, 1288 (2020).
[43] M. Gessner, C. Fabre, and N. Treps, Superresolution Limits from Measurement Crosstalk, Phys. Rev. Lett. **125**, 100501 (2020).
[44] G. Sorelli, M. Gessner, M. Walschaers, and N. Treps, Optimal Observables and Estimators for Practical Superresolution Imaging, Phys. Rev. Lett. **127**, 123604 (2021).
[45] J. O. de Almeida, J. Kołodyński, C. Hirche, M. Lewenstein, and M. Skotiniotis, Discrimination and estimation of incoherent sources under misalignment, Phys. Rev. A **103**, 022406 (2021).
[46] J. Řehaček, Z. Hradil, B. Stoklasa, M. Paúr, J. Grover, A. Krzic, and L. L. Sánchez-Soto, Multiparameter quantum metrology of incoherent point sources: Towards realistic superresolution, Phys. Rev. A **96**, 062107 (2017).
[47] W. Larson and B. E. A. Saleh, Resurgence of Rayleigh's curse in the presence of partial coherence, Optica **5**, 1382 (2018).
[48] K. Liang, S. A. Wadood, and A. N. Vamivakas, Coherence effects on estimating two-point separation, Optica **8**, 243 (2021).
[49] T. Linowski, K. Schlichtholz, G. Sorelli, M. Gessner, M. Walschaers, N. Treps, and Łukasz Rudnicki, Application range of crosstalk-affected spatial demultiplexing for resolving separations between unbalanced sources, arXiv:2211.09157 (2022).
[50] T. Tan, K. K. Lee, A. Ashok, A. Datta, and B. A. Bash, Robust adaptive quantum-limited super-resolution imaging, in *Proceedings of the 2022 56th Asilomar Conference on Signals, Systems, and Computers Pacific Grove, CA* (IEEE, Piscataway, NJ, 2022), pp. 504–508.
[51] B. Wang, L. Xu, J. chi Li, and L. Zhang, Quantum-limited localization and resolution in three dimensions, Photon. Res. **9**, 1522 (2021).

[52] S. Kurdziałek, and R. Demkowicz-Dobrzański, Measurement Noise Susceptibility in Quantum Estimation, Phys. Rev. Lett. **130**, 160802 (2023).

[53] Y. L. Len, C. Datta, M. Parniak, and K. Banaszek, Resolution limits of spatial mode demultiplexing with noisy detection, Int. J. Quantum. Inform. **18**, 1941015 (2020).

[54] C. Lupo, Subwavelength quantum imaging with noisy detectors, Phys. Rev. A **101**, 022323 (2020).

[55] C. Oh, S. Zhou, Y. Wong, and L. Jiang, Quantum Limits of Superresolution in a Noisy Environment, Phys. Rev. Lett. **126**, 120502 (2021).

[56] C. K. Hong, Z. Y. Ou, and L. Mandel, Measurement of Subpicosecond Time Intervals Between Two Photons by Interference, Phys. Rev. Lett. **59**, 2044 (1987).

[57] M. O. Scully and M. S. Zubairy, *Quantum Optics* (Cambridge University, New York, 1997).

[58] R. Loudon, *The Quantum Theory of Light* (Oxford University, New York, 2000).

[59] I. Aharonovich, D. Englund, and M. Toth, Solid-state single-photon emitters, Nat. Photonics **10**, 631 (2016).

[60] S. I. Bogdanov, A. Boltasseva, and V. M. Shalaev, Overcoming quantum decoherence with plasmonics, Science **364**, 532 (2019).

[61] F. W. Sun and C. W. Wong, Indistinguishability of independent single photons, Phys. Rev. A **79**, 013824 (2009).

[62] P. Kaer, N. Gregersen, and J. Mork, The role of phonon scattering in the indistinguishability of photons emitted from semiconductor cavity qed systems, New J. Phys. **15**, 035027 (2013).

[63] M. Parniak, S. Borówka, K. Boroszko, W. Wasilewski, K. Banaszek, and R. Demkowicz-Dobrzański, Beating the Rayleigh Limit Using Two-Photon Interference, Phys. Rev. Lett. **121**, 250503 (2018).

[64] S. Unsleber, D. P. S. McCutcheon, M. Dambach, M. Lermer, N. Gregersen, S. Höfling, J. Mørk, C. Schneider, and M. Kamp, Two-photon interference from a quantum dot microcavity: Persistent pure dephasing and suppression of time jitter, Phys. Rev. B **91**, 075413 (2015).

[65] E. Schöll, L. Schweickert, L. Hanschke, K. D. Zeuner, F. Sbresny, T. Lettner, R. Trivedi, M. Reindl, S. F. Covre da Silva, R. Trotta, J. J. Finley, J. Vučković, K. Müller, A. Rastelli, V. Zwiller, and K. D. Jöns, Crux of Using the Cascaded Emission of a Three-Level Quantum Ladder System to Generate Indistinguishable Photons, Phys. Rev. Lett. **125**, 233605 (2020).

[66] H. Ollivier, S. E. Thomas, S. C. Wein, I. M. de Buy Wenniger, N. Coste, J. C. Loredo, N. Somaschi, A. Harouri, A. Lemaitre, I. Sagnes, L. Lanco, C. Simon, C. Anton, O. Krebs, and P. Senellart, Hong-Ou-Mandel Interference with Imperfect Single Photon Sources, Phys. Rev. Lett. **126**, 063602 (2021).

[67] A. J. Bowman, B. B. Klopfer, T. Juffmann, and M. A. Kasevich, Electro-optic imaging enables efficient wide-field fluorescence lifetime microscopy, Nat. Commun. **10**, 4561 (2019).

[68] D. V. Widder, *The Laplace Transform (PMS-6)*, Vol. 61 (Princeton University, Princeton, NJ, 2015).